OUT-OF-PLANE BEHAVIOUR OF SINGLE-WYTHE 3D PRINTED CONCRETE WALL PANELS WITH NEAR SURFACE MOUNTED REINFORCEMENT

Hentschel[1], Alexander, Fam[2], Amir, and Woods[3], Joshua

[1]Graduate Student, Department of Civil Engineering, Queen's University, Ellis Hall, Kingston, ON K7L 3N6, Canada. E-mail: alexander.hentschel@queensu.ca
[2]Canada Research Chair and Vice Dean (Research), Department of Civil Engineering, Queen's University, Ellis Hall, Kingston, ON K7L 3N6, Canada. E-mail: amir.fam@queensu.ca
[3]Assistant Professor, Department of Civil Engineering, Queen's University, Ellis Hall, Kingston, ON K7L 3N6, Canada. E-mail: joshua.woods@queensu.ca (Corresponding Author)

ABSTRACT

Additive manufacturing of low-rise residential and commercial buildings using printed cementitious materials, a technology that is commonly referred to as 3D concrete printing (3DCP), is now being deployed at scale across North America. A significant challenge in expanding the use of 3DCP is determining an efficient and effective approach to incorporate longitudinal reinforcement into walls. This study proposes the use of near surface mounted (NSM) reinforcement in 3DCP walls and evaluates the structural behaviour of single-wythe 3DCP wall panels under out-of-plane loading through experimental testing. An innovative wet-formed groove technique for the NSM bar is proposed, which involved forming the groove during the printing process, which is compared to traditional saw-cut grooves. The work also investigates the influence of reinforcement type (steel and GFRP), NSM bonding material type (epoxy, cementitious mortar, and concrete), and reinforcement ratio on wythe behaviour. Digital image correlation (DIC) is used to capture full-field strain distributions in the wall panels as well as crack widths. Results show that the use of NSM reinforcement is effective at enhancing the flexural stiffness, strength, and ductility and 3DCP wall panels. Steel-reinforced walls failed due to flexural yielding while GFRP-reinforced walls failed due to rupture of the reinforcement or bond failure. No significant differences were observed between the performance of wet-formed or saw cut grooves, suggesting the potential for speeding up construction. GFRP-reinforced panels with a 0.6% reinforcement ratio failed by rupture of the GFRP bars, while those with a 0.8% ratio experienced bond failure for both epoxy and mortar materials, although epoxy adhesive enabled a 40%

increase in load compared to cementitious mortar. The experimental results are compared with existing approaches to predict their flexural performance, and the results show the strength can be predicted within 10% on average. A recommended design thickness is proposed given the inherent variability in the thickness of 3D printed concrete wythes, which improves strength predictions.

Keywords: 3D concrete printing, additive manufacturing, walls, near surface mounted reinforcement, out-of-plane loading, fibre reinforced polymer, digital image correlation

INTRODUCTION

Shortages of skilled labour and the need to improve construction productivity have driven demand to innovative the way that homes and buildings are constructed around the globe. Historically, construction has been a field that has been slow to adapt to advances in technology in comparison to other fields, for example, industrial manufacturing, which is due in part to the challenging site conditions in construction and the uniqueness of each project [1]. Despite these challenges there has been increasing focus in recent years on technologies that can improve the efficiency of construction using robotic systems. One such technology is 3D concrete printing (3DCP), which uses a robotic arm or gantry system to extrude fresh concrete using an additive manufacturing approach. This approach permits construction of concrete walls or columns without the need to temporary formwork or as many skilled labourers as are required using conventional construction practices, resulting in the potential for improved construction efficiency and reduced waste when compared with traditional construction methods [2,3].

Despite the promise of 3DCP technology for the construction of homes and buildings, it is still in its infancy, and many questions remain surrounding its performance as a structural material [3]. This work has been summarized in several state-of-the-art reviews [4-6]. Recent research pertaining to the mechanical behaviour of 3DPC have largely focused on the performance at the material level, including studying the flowability/curing requirements, different mix constituents, compressive and tensile strength, and the inter-layer bond behaviour [4-6].

In comparison, there have been fewer studies focused on examining the structural behaviour of 3DCP structural components or sub-assemblies (e.g., walls or columns). This work has included experimental testing to evaluate wall behaviour under concentric axial compression [7-9], eccentric axial compression [10], and the in-plane lateral cyclic loading [11-13]. One aspect that varies amongst these studies and continues to be a challenge in 3DCP is the incorporation of longitudinal reinforcement. Particularly for taller structures or structures in regions of high seismicity, the incorporation of longitudinal reinforcement is critical to meet ultimate limit states resistance requirements and also to ensure ductile behaviour during an earthquake. There is a significant body of evidence on the poor seismic performance of unreinforced masonry structures under in-plane [14,15] and out-of-plane loads [16], which would also apply to the performance of unreinforced 3DCP structures.

While it is commonly recognized in the literature that there is a need to incorporate longitudinal reinforcement in 3DCP elements there is no consensus on how this can be efficiently achieved in practice [17,18]. Because of the nature of 3DCP construction in which a nozzle sequentially extrudes the layers in a structural component vertically, the conventional approach of placing vertical reinforcement prior to casting the concrete would interfere with the printer, and consequently, this approach cannot be directly transferred to 3DCP construction. Recent state-of-the-art reviews have highlighted that reinforcement can be readily integrated between printed layers when aligned parallel to the printing plane while maintaining the same characteristics in terms of bond strength and pull-out strength [19-21], however, these same techniques cannot be used for reinforcement perpendicular to the printed layers.

To address the challenge of incorporating longitudinal reinforcement in 3DCP construction, there have been several proposed solutions in the literature, including placement of reinforced inside printed cavities, either before or after printing is complete, and then filling the cavities with grout [11]. This approach mimics what is currently done in masonry construction and despite its effectiveness, it reduces the efficiency of 3DCP because of the time required to place reinforcement and grout cavities. Furthermore, it also results in reinforcement that is located inefficiently in the cross-section (near the neutral axis) and often requires splicing of reinforcement over the element height during printing. Alternatively, more novel approaches researchers have focused on include directly printing material around longitudinal reinforcement, either through a multi-nozzle approach [22] or by using shotcrete [23], resulting in a structural component that is more representative of reinforced concrete. The disadvantage of this approach is that it is not compatible or easily applied to commercial 3DCP technology being used in practice. Alternatively, work has also focused on printing of modular components that are joined together using longitudinal reinforcement [19]. While potentially effective, questions remain surrounding the applicability of this approach at scale, as it does not follow the typical construction sequence adopted in practice. Finally, more innovative approaches have included printing the concrete and steel reinforcement simultaneously using additive manufacturing techniques [24] or using modular steel elements [25]. While these techniques have the potential to eliminate the need altogether for human labour, they are not sufficiently developed to be rapidly applied at-scale. A review of the literature has identified that there is an ongoing need to develop novel reinforcing solutions for 3DCP structures.

To the authors' knowledge, this is the first study of its kind to examine the use of near surface mounted (NSM) reinforcement for 3D printed concrete structures. The specific objective of this research is to: (1) study the feasibility of using both wet-formed grooves as well as cut grooves for the placement of longitudinal reinforcement in 3DCP walls, (2) study the influence of reinforcement type, reinforcement ratio, and type of bonding material used to install the NSM reinforcement in terms of strength and failure mode, (3) Use digital image correlation to study the strain (and stress) distributions in 3DCP wall panels with naturally varying geometry, and (4) study how the variable geometry of the layered 3DCP walls influences their flexural strength and compare the experimental results with theoretical predictions.

EXPERIMENTAL PROGRAM

The experimental program consisted of 16 single-wythe wall panels with NSM reinforcement. The specimens included those with varying groove forming techniques (e.g., wet-formed and saw-cut), reinforcing bar types (e.g., steel and GFRP reinforcement), adhesive material (e.g., epoxy, mortar, and concrete), and reinforcement ratio.

Wall Panel Specimens

Figure 1 shows the geometry of the wall panel specimens and the larger sections from which they were cut. The single-wythe wall panels measured 1650 × 600 × 50 mm ($l \times w \times h$). While 3DCP walls are typically double-wythe with crossties and an insulation layer in between, the degree of composite action is generally very small. Consequently, it is not unusual for each wythe to experience both compressive and tensile flexural stresses (i.e. each has its own neutral axis) as in some precast sandwich panels [26]. As such, this study is focused on single-wythe specimens.

To fabricate the wall panels, a three-axis gantry-type extrusion system (COBOD BOD2) was used. To enable printing of the wall and to ensure they remained stable during fabrication, four four-sided towers were printed and the individual wall panels were cut from the towers after they were cured and shipped to the laboratory. The printer speed was approximately 100 mm/s, which resulted in a layer time of approximately 12 minutes. The walls were printed in two phases, which included first printing to a height of approximately 500 mm, followed by a second phase the next day to a final height of 1650 mm. This means that there was a cold joint in the wall panels at approximately 30% of the wall height, the structural implications of which are discussed in subsequent sections of this paper. While the construction in two stages occurred in this case due to some challenges with the equipment, it is a realistic scenario that could occur in the field for the same reason or between work shifts.

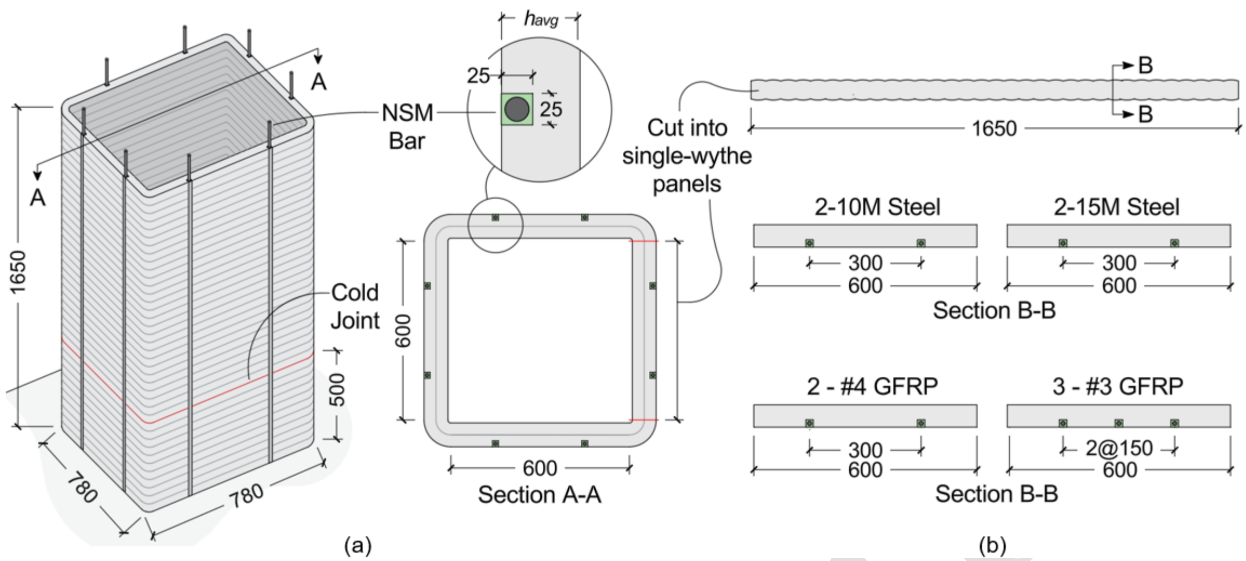

Figure 1. Specimen geometry: (a) four-sided 3DCP towers, (b) single-wythe panel cross-sections.

To reinforce the wall panels, an NSM technique was adopted. While the use of NSM reinforcement in repair or strengthening applications is a concept that has been extensively applied to reinforced concrete structures [27], however, its application to 3DCP elements has not been studied in the literature. Two techniques for installing the NSM reinforcement were considered in this study. The first method is novel and is intended for rapid on-site installation specific to 3DCP construction. This technique, referred to as a wet-formed groove, involves forming a groove in the printed material during the printing process prior to the material reaching its hardened state. The advantage of using a wet-formed groove is that the reinforcement can be installed immediately on-site and could be bonded using the same material that its extruded from the printer, something that is also considered in this study. The second technique for installation of NSM reinforcement considered follows the traditional method used in the literature for reinforced concrete or masonry applications and involves cutting a groove after the concrete is cured.

Figure 1(b) shows the cross-sections of the reinforced wall panels tested in this study. Different reinforcement types, NSM bonding material types, and reinforcement ratios were considered in this study, which are summarized in Table 1. The first series of specimens were reinforced with steel rebar and included either 2-10M ($d_b = 11.3$ mm, $A_r = 200$ mm^2) or 2-15M ($d_b = 16.0$ mm, $A_r = 400$ mm^2) bars, resulting in reinforcement ratios (ρ = A_r/bd) of 0.88% and 1.75%, respectively, based on the nominal effective depth d of 38 mm (nominal h = 50 mm minus 12.5 mm cover (Fig. 1(a)). The second series had GFRP reinforcing bars, with either 3-#2 bars (d_b = 6.2 mm, A_r = 90.6 mm^2) or 2-#3 bars (d_b = 9.5 mm, A_r = 142 mm^2), resulting in reinforcement ratios of 0.40% and 0.62%, respectively. The GFRP reinforcement ratios were established based on equivalent ultimate forces in the reinforcement as the steel reinforcement (A_rf_r), based on the design ultimate and yield strengths of the two materials (see materials sections). These forces are 72.5 kN and 80 kN for the GFRP and steel at the lower reinforcement ratios of 0.4% and 0.88%, respectively, while they were 142 kN and 160 kN for the GFRP and steel at the higher reinforcement ratios of 1.75% and 0.62%, respectively.

Table 1. Test matrix and specimen geometry

Name	Groove Type	Bond Material	NSM Bar	f_y (MPa)	No - Size of Bars	d_b (mm)	ρ (%)	h_{min} (mm)	h_{avg} (mm)
GFRP-0.4-E	Saw-cut	Epoxy	GFRP	-	3 - #2	6.2	0.40	50	62
GFRP-0.6-E-1				-	2 - #3	9.5	0.62	46	56
GFRP-0.6-E-2				-	2 - #3	9.5	0.62	48	63
Steel-0.9-E-1	Saw-cut	Epoxy	Steel	509	2 - 10M	11.3	0.88	46	59
Steel-0.9-E-2				521	2 - 10M	11.3	0.88	38	51
Steel-1.8-E-1				524	2 - 15M	16.0	1.75	42	57
Steel-1.8-E-2				522	2 - 15M	16.0	1.75	43	55
GFRP-0.4-M	Saw-cut	Mortar	GFRP	-	3 - #2	9.7	0.40	45	59
GFRP-0.6-M-1				-	2 - #3	9.7	0.62	51	64
GFRP-0.6-M-2				-	2 - #3	9.7	0.62	54	55
Steel-0.9-M-1	Saw-cut	Mortar	Steel	518	2 - 10M	11.3	0.88	47	58
Steel-0.9-M-2				454	2 - 10M	11.3	0.88	48	56
Steel-1.8-M-1				417	2 - 15M	16.0	1.75	38	54
Steel-1.8-M-2				433	2 - 15M	16.0	1.75	44	54
Steel-0.8-C-1	Wet-formed	Concrete	Steel	503	2 - 10M	11.3	0.88	48	60
Steel-0.8-C-2				499	2 - 10M	11.3	0.88	45	57

Note: f_y – yield stress, d_b – bar diameter, h_{min} – minimum wythe thickness, h_{avg} – average wythe thickness

Three different materials were used to bond NSM reinforcement into the groove, depending on the specimen (see Table 1). This included either: (1) the 3DCP material taken from the printer during fabrication of the four-sided towers, which was used for installation of bars into wet-formed grooves and hereafter referred to as concrete, (2) a cementitious mortar (Sika Monotop 623 F) used with saw-cut grooves, or (3) an epoxy adhesive (SikaDur30) used with saw-cut grooves. Different bond materials were selected to examine the influence of varying bond properties, as well as ranging costs. The use of concrete from the printer would likely result in much lower costs when compared to an off-the-shelf adhesive product, especially when coupled with the wet-formed groove technique, which requires significantly less on-site labor when compared with traditional saw cutting techniques.

The naming convention used for the specimens included first the NSM reinforcement type (e.g., GFRP or Steel), followed by the reinforcement ratio (e.g., 0.*XX*), NSM bonding material type (e.g., E – epoxy, M – mortar, C – concrete), and finally the specimen repetition (if applicable). For example, specimen GFRP-0.4-G-2 had GFRP reinforcement, a reinforcement ratio of approximately 0.4%, used grout as the adhesive material for the NSM bars, and was the second repetition.

Specimen Fabrication

Figure 2 highlights select steps in the specimen construction process. Generally, fabrication of the single-wythe wall panels included printing of the towers, installation of the NSM reinforcement, and extracting the single-wythe panels using a wet saw. The reinforcement was installed prior to cutting the wall panels from the towers to simulate the realistic conditions under which the NSM reinforcement would be installed in the field, which required consideration for vertical application of the adhesive.

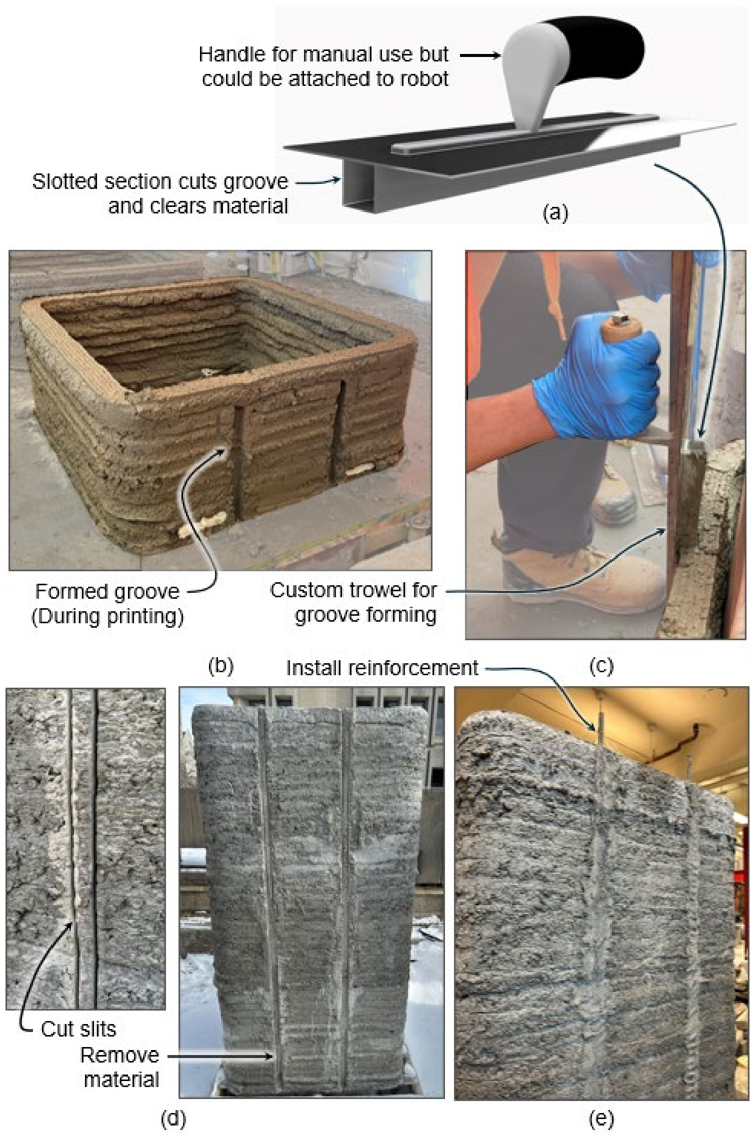

Figure 2. Specimen fabrication: (a) custom trowel for wet-formed groove, (b) four-sided 3DCP tower, (c) formation of wet-formed groove, (d) process for saw cut groove, (e) installation of NSM bars.

Installation of the NSM reinforcement began with formation of the grooves, which was either wet-formed during printing or saw-cut after curing. For the wet-formed grooves, a specialized trowel designed for this application, shown in Figure 2(b), which has a protruding rectangular section that is used to form a groove while the concrete was still workable. The saw-cut grooves were formed by first cutting parallel grooves measuring ~3 mm wide and ~25 mm apart, vertically, along the length of the panels using a concrete saw. Concrete material between the saw cuts was then removed using a chisel (Figure 2(d)).

Irrespective of groove type, the NSM reinforcement installation was completed in four stages: (1) the grooves were cleaned to remove any leftover debris, (2) the groove was partially filled (half of the depth) with either concrete, epoxy, or mortar (depending on the specimen type), (3) the reinforcement was then placed and pressed into the grooves and alignment along the groove length was ensured, (4) the remaining half of the groove was filled with the same material, and (5) the specimens were left to cure for at least 7 days before handling. After the reinforcement had been installed, the panels were cut from the box sections into single-wythe panels for testing. The as-built dimensions of the panels were then assessed. Because of the nature of the 3DCP fabrication process, there was some variability in the layer width along the length of the specimens due to localized bulging caused by the printing of subsequent layers, which exerts pressure on the underlying layer. This geometric irregularity complicates the definition of the thickness of the wall panel, which was non-uniform along the length.

Figure 3 shows a typical section of a 3DCP wall panel in this study. To determine the thickness along the length of the panels, an image processing technique was developed to accurately measure the cross-sectional dimension of each wall panel. The technique involved first taking an image of the side of each wall panel, an example of which is shown in Figure 3(a). The image was then converted to a binary black and white image (Figure 3(b)) and imported into the Inkscape software [28]. An automatic contour matching algorithm was then used to determine the contour of the wall panel (Figure 3(c)). Based on the contour and the scale in the original image, the thickness of the panel along its length was determined, including both the minimum thickness (h_{min}) and average thickness (h_{avg}) as well as the minimum and average depths to the reinforcement (d_{min}) and (d_{avg}), respectively. The results of this technique are summarized in Table 1 and are used in the theoretical assessment of the strength of the specimens in a subsequent section of this paper.

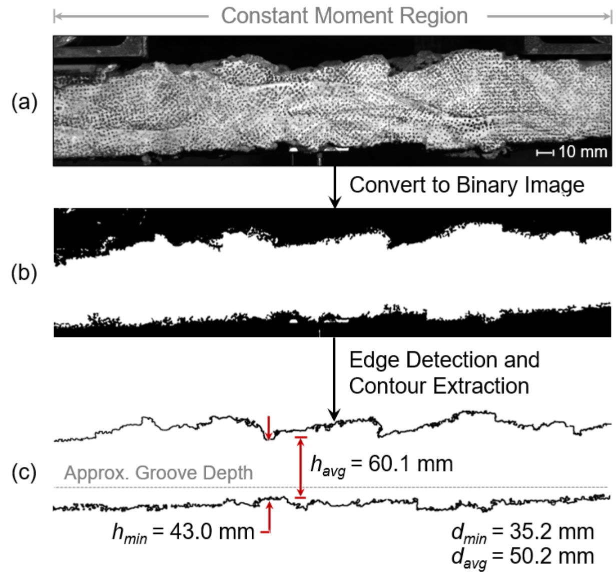

Figure 3. Process to determine the minimum and average member height along the length of the 3DCP wall panel: (a) original image, (b) binary image, (c) extracted contour and dimensions.

Material Properties

3D Printed Concrete: One of the challenges associated with the use of 3D printed concrete is determining the properties of the materials, which similar to masonry, should be based on the in-situ geometry of the material (i.e., in printed layers for 3DCP), because this can influence the strength [29]. To evaluate this assumption, material properties in this study were assessed both using the traditional approaches that would be used in reinforced concrete, including mold cast cylinders and prisms, in addition to 3DCP specimens that were saw-cut from the wall panel material. It is noted that the mold cast samples were prepared on the same day as the 3DCP materials and the cast concrete was taken directly from the printer head, such that it would have material properties that were as close as possible at the printed materials.

The 3DCP material used in this study were proprietary to the manufacturing company, and thus, detailed mix design information is not available. However, generally, the mix included a cement content from 400-600 kg/m^3, fine aggregate, superplasticizer, accelerator, and a hardener at the nozzle. The concrete had maximum coarse aggregate size of 6.4 mm, was air entrained (6-8%), and included synthetic monofilament microfiber to reduce plastic shrinkage cracking.

To identify the compressive strength of the concrete cylindrical specimens (100 × 200 mm) were first tested under uniaxial compression, following the procedures specified in ASTM C39/C39M [30]. This resulted in a compressive strength of 64.9 MPa (standard deviation (SD) = 3.19 MPa). To better reflect the material behaviour of printed concrete, additional compression tests were carried out on prisms, which were saw-cut from the wall samples as indicated earlier. The prisms were nominally 50 mm × 50 mm and were 155 mm tall, representing approximately three layers of printed material. The average compressive strength of the 3DCP prisms was 44.1 MPa (SD = 6.61 MPa), which is 32 % lower than the mold cast cylinders. This phenomena between the strength of mold-cast and printed concrete materials in compression has been noted by other researchers in the literature [29].

In addition to compressive strength, the modulus of rupture of the material was also evaluated through tests on conventional mold cast prisms as well as prisms that were saw-cut from a 3DCP element. The modulus of rupture specimens followed the guidelines outlined in ASTM C78/C78M [31] and the cast concrete prisms were 80×80×280 mm, while the printed concrete prisms had nominal dimensions of 50×50×240 mm. The modulus of rupture of the cast and printed concrete did not vary significantly as the average modulus of rupture in the cast concrete prisms was 5.97 MPa (SD = 0.52 MPa) compared to 5.68 MPa (SD = 0.97 MPa) in the printed mortar prisms. While the averages are similar, there was more variation in the results from the printed concrete, which is attributed to the variation in the cross-section of the prisms along their length.

NSM Reinforcement Bonding Materials: three different materials were used to bond the NSM reinforcement in the concrete, which depended on the type of groove (i.e., formed or cut). For the wet-formed grooves during printing, the bars were installed into the grooves using printed material during specimen fabrication. Consequently, the material has the same properties that were noted in the previous section. For the cut grooves, which were formed after the concrete had cured, the effectiveness of both a cementitious mortar as well as an epoxy adhesive were examined. The cementitious grout (Sika MonoTop 623 F) is a one-component, polymer modified, fibre-reinforced cementitious mortar intended for vertical and overhead repair applications. The material has a pull-off strength greater than 3 MPa, an elastic modulus of 18 GPa, and a flexural tensile strength of 10.1 MPa at 28-days according to the manufacturer [32].

The epoxy adhesive (SikaDur 30) used to bond the NSM reinforcement is a two-component epoxy paste adhesive intended for bonding of composite materials to concrete or masonry and is suitable for use in vertical or overhead applications. The product has a modulus of elasticity of 2.69 GPa, a tensile strength of 24.8 MPa, and a shear strength of 15 MPa [33].

GFRP Reinforcement: the #2 GFRP reinforcement (V-ROD Grade I) was a sand-coated bar with A_b = 31.6 mm^2 cross-sectional area and had a reported elastic modulus of 40 GPa, a minimum tensile strength of 800 MPa, and an ultimate strain of 2.1% [34]. The #3 GFRP reinforcement (MST-Bar Grade III) was a ribbed bar with A_b = 71 mm^2 cross-sectional area and had a reported elastic modulus of 60 GPa, a minimum tensile strength of 1000 MPa, and an ultimate strain of 1.7 % [35].

Steel Reinforcement: the steel reinforcement was grade 400W and included bar sizes of 10M and 15M with A_b = 100 and A_b = 200 mm^2, respectively. Tensile tests on steel bars taken from the test samples were conducted according to the procedures outlined in ASTM E8/E8M [36]. Based on the results of the coupon tests, the steel reinforcement had average yield stresses (f_y) as summarized in Table 1. It is noted that the steel reinforcement came from different batches of material, and so, repeated coupon tests were conducted on samples taken from each wall panel.

Test Setup and Instrumentation

The reinforced 3DCP wall panels were tested in out-of-plane bending in a four-point bending configuration, with simple boundary conditions and point loads located at one-third of the span length. Figure 4 shows the experimental test setup. The load was applied using a hydraulic actuator (+/- 500 kN, +/- 75 mm) through a steel spreader beam. To ensure the panel was level at the support and load locations, grouted pads were used to form a level surface (as noted in Figure 4). This was required to compensate for the variability in the thickness of the 3DCP along the panel length, as discussed previously.

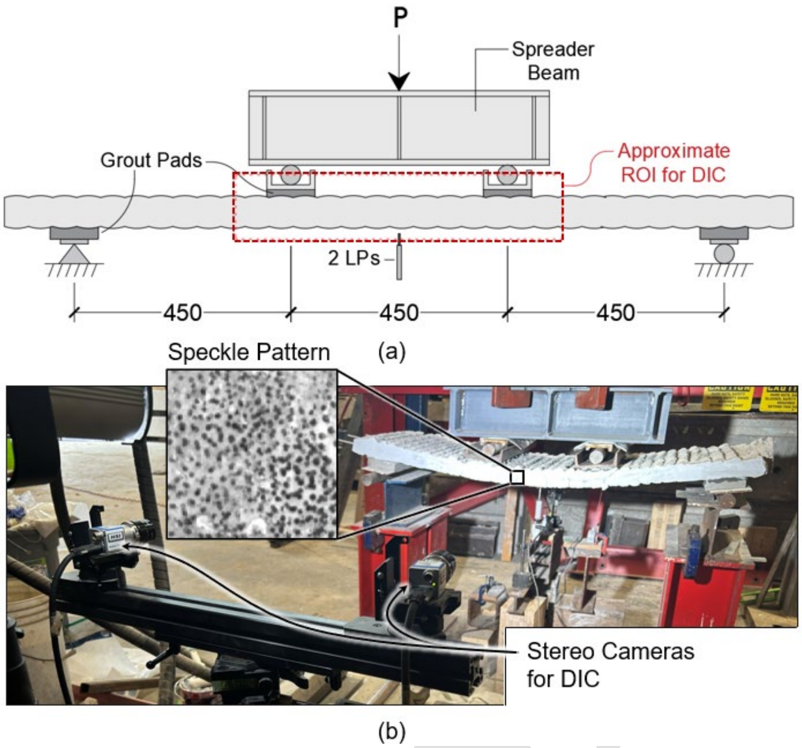

Figure 4. Typical experimental test setup and digital image correlation configuration

The panels were loaded in displacement control at an initial rate of 0.5 mm/min up to yielding of the reinforcement (in steel reinforced specimens) or significant cracking (in GFRP reinforced specimens). Subsequently, the loading rate was increased to 1.0 mm/min up to the end of the test. The test was stopped at the onset of brittle failure or a midspan deflection of ~80 mm (corresponds to deflection of L/20), whichever occurred first.

To measure the structural response of the panels, two linear potentiometers were placed at midspan to measure the deflection. To track crack formation, measure crack widths, and estimate tensile/compressive strain in the constant moment region, digital image correlation (DIC) was employed. Due to the variability in the thickness of the panel along the length, DIC was particularly advantageous in this application because of the potential for full-field displacement/strain results, eliminating the need for a priori knowledge of the locations of maximum and minimum strain. The process for DIC analysis included first painting the surface of the panel with a white basecoat and speckle pattern. Two cameras (5 MP) were focused on the constant moment regions of the panel (i.e., central ~600 mm) and images were taken at 0.2 Hz throughout the test. Post-processing of the images was conducted using VIC3D analysis software [37].

EXPERIMENTAL RESULTS AND DISCUSSION

Table 2 summarizes the key structural response parameters for the 3DCP wall panels tested in this study, including the initial stiffness (k_i), cracking load (P_{cr}), deflection at yield (Δ_y), maximum load (P_{max}), deflection at ultimate (Δ_{ult}), and average crack spacing (s_{avg}). The initial stiffness was determined by fitting a line through the load versus deflection response of the specimens between 10% of the maximum load and the cracking load. The average crack spacing was determined using DIC analysis, the results of which are discussed in a subsequent section of this paper.

Table 2. Summary of test results

Specimen Name	k_i (kN/mm)	P_{cr} (kN)	Δ_y (mm)	P_{max} (kN)	Δ_{ult} (mm)	s_{avg} (mm)	Failure Mode
GFRP-0.4-E	3.19	6.93	-	14.3	81.3	100	Rupture
GFRP-0.6-E-1	1.75	7.18	-	20.4	76.6	140	Bond
GFRP-0.6-E-2	2.28	8.63	-	24.4	71.3	92	Bond
Steel-0.9-E-1	4.01	5.49	14.1	20.2	41.3	-	Yield
Steel-0.9-E-2	3.49	9.65	9.9	19.2	82.5	147	Yield
Steel-1.8-E-1	3.28	5.15	17.3	37.9	75.8	-	Yield+Bond
Steel-1.8-E-2	3.73	5.44	13.7	33.8	69.5	106	Yield
GFRP-0.4-M	3.16	2.78	-	16.8	79.1	114	Rupture
GFRP-0.6-M-1	3.84	4.12	-	12.9	43.9	157	Bond
GFRP-0.6-M-2	2.21	3.23	-	13.4	41.6	203	Bond
Steel-0.9-M-1	3.87	5.22	16.0	19.2	16.0	176	Bond
Steel-0.9-M-2	3.47	5.96	13.0	18.1	17.7	125	Yield
Steel-1.8-M-1	4.38	5.68	13.4	29.9	14.2	-	Bond
Steel-1.8-M-2	3.28	9.33	15.3	29.3	24.0	-	Bond
Steel-0.9-C-1	3.65	5.49	10.4	20.0	62.4	117	Yield
Steel-0.9-C-2	2.41	6.41	12.5	15.5	64.6	-	Yield

Load-Deflection Behaviour and Failure Modes

Figure 5 shows the load-deflection relationship for the GFRP-reinforced wall panels tested in this study. The wall panels exhibit an initial elastic response followed by an abrupt change in the slope at the onset of cracking. The initial stiffness and cracking load were found to be variable amongst the tested wall panels, even for nominally identical specimens. While past research has shown that the cracking load can vary significantly in reinforced concrete beams (Kim et al. 2010), the observed differences are also attributed to the irregularity of the section along the length resulting in variations in the thickness and the depth of the reinforcement as well as the NSM bonding material. For example, comparing the wall panels with #3 GFRP reinforcement (ρ = 0.6 %) with mortar as the NSM bond material in Figure 5(c), the results show that the specimens had a cracking strength that were 25 % different between two nominally identical specimens, which is, in part, attributed to differences in geometry, as the average thickness (h_{avg}) varied between the two panels by 15 % (panel with larger average thickness had higher cracking load). Comparing epoxy and mortar NSM bonding materials, the panels that used mortar had a 50 % lower cracking strength (on average) when compared to the specimens with epoxy, even though the specimens had comparable minimum and average thicknesses (listed in Table 1). These differences are attributed to the higher tensile strength of the epoxy material, indicating that both geometry and NSM bonding material influence the panel behaviour.

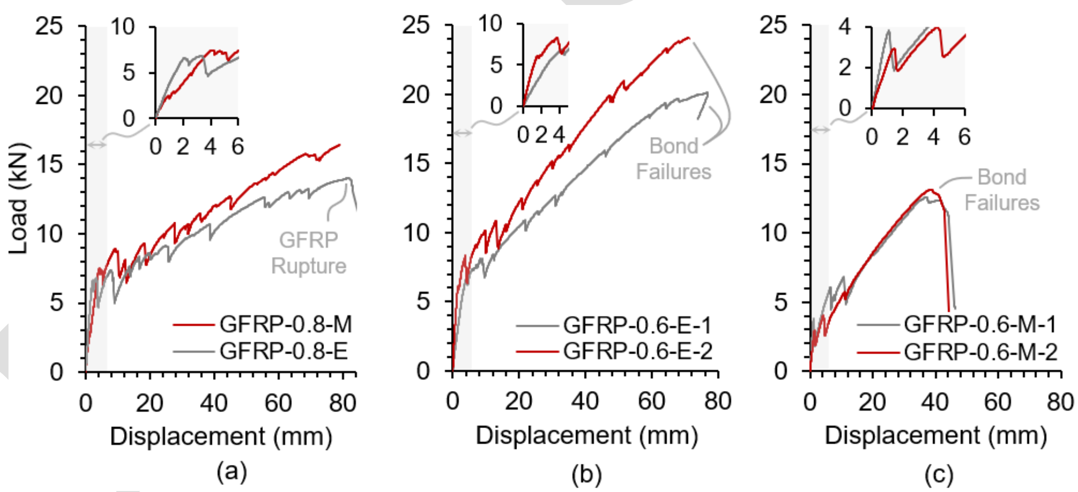

Figure 5. Load versus deflection behaviour of the GFRP reinforced wall panels with: (a) ρ = 0.4% (#2 GFRP bars), (b) ρ = 0.6% (#3 GFRP bars) with epoxy adhesive and (c) ρ = 0.6 % with cementitious mortar bonding material. All specimens had saw-cut grooves.

After cracking, the wall panels exhibit a reduced stiffness, including several load drops, which are indicative of the formation of new cracks along the member length. The panels that used epoxy adhesive to bond the NSM reinforcement were able to achieve very large displacements (>*L*/20) prior to failure. As expected, increasing the reinforcement ratio from 0.4% to 0.6% resulted in a 56% increase in the ultimate load carrying capacity of the wall panels on average. Comparing the use of mortar and epoxy to bond the NSM reinforcement, for a reinforcement ratio of 0.4%, the ultimate displacement and load-carrying capacity were within 5% of one another for the nominally identical panels. In contrast, the wall panels that had a reinforcement ratio of 0.6% had a decrease of 40% in the ultimate displacement (*L*/40) and ultimate load-carrying capacity, when compared to the nominally identical wall panels that used epoxy to bond the NSM reinforcement. This is attributed to the higher bond stresses for the larger bar size in the beams with the higher reinforcement ratio. Generally, it can be concluded that the two bonding methods (epoxy and mortar) enabled small GFRP reinforcement ratios (e.g. 0.4% in this study) to achieve rupture, however, bond failure occurred for larger reinforcement ratio (0.6% in this study) with both epoxy and mortar, except that with epoxy, it occurred at a 72% higher load.

Figure 6 compares the load-deflection behaviour of the steel-reinforced wall panels. The results show once again that the panels exhibit a behaviour that is similar to what would be expected from a steel reinforced concrete beam, including an abrupt change in stiffness at the cracking load, followed by an elastic cracked response up to the yield load. The results in Table 2 once again show some discrepancies between the cracking loads of the specimens, which is attributed to variations in the geometry of the specimens and NSM bond material. Panels with a reinforcement ratio of 0.9% were able to achieve very large deflections and exhibit a ductile load-deflection response. The wall achieved an average ultimate load of 18.7 kN, which was roughly 3-4 times the cracking load. Very similar behaviour was observed in the wall with a reinforcement ratio of 1.8% that used epoxy adhesive. In contrast, wall panels with a reinforcement ratio of 1.8% that used mortar achieved an ultimate deflection that was approximately 50% of those with the smaller reinforcement ratio, but with an average load-carrying capacity of 32.7 kN. The lower displacement capacity of these specimens is attributed to the onset of a brittle failure mode, something that is discussed in the next section of this paper.

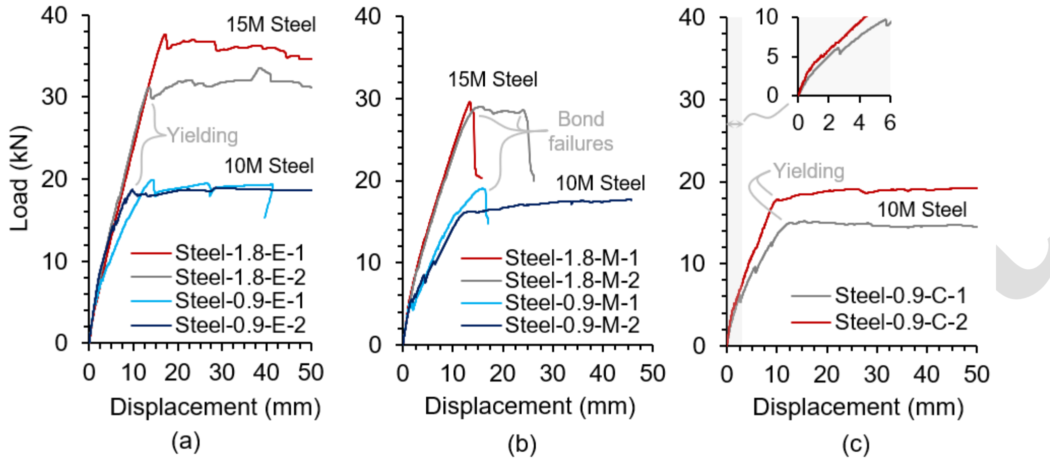

Figure 6. Load versus deflection behaviour of the steel reinforced wall panels with: (a) epoxy adhesive (saw-cut groove) (b) mortar (saw-cut groove), and (c) concrete (wet-formed groove).

Comparing the behaviour of the specimens that had a wet-formed groove and used the printing material to bond the NSM reinforcement, shown in Figure 6(c), the results show that the walls had a strength that was comparable (average capacity of 17.8 kN compared with 19.2 kN) to those that used mortar or epoxy adhesive to bond the NSM reinforcement. The smaller load carrying capacity of wall panel Steel-0.9-C-2, which yielded at a 10 % lower than its counterpart, is attributed to the presence of a very thin section within the constant moment region, which had a minimum thickness that was approximately 10 % smaller than its counterpart. This resulted in localized yielding and a smaller force couple between the steel reinforcement in tension and the concrete in compression. Generally, it can be concluded that all bonding methods (epoxy, mortar and concrete) enable small steel reinforcement ratios (e.g. 0.9% in this study) to achieve yield strength, however, for larger reinforcement ratio (1.8% in this study) only epoxy enabled steel to sufficiently yield considering that concrete bonding material was not tested for the larger ratio. Nonetheless, these results suggest that the wet-formed groove during printing and using the printed concrete material to bond the NSM reinforcement can be an effective approach to reinforce a 3DCP wall, something that has several advantages over traditional techniques, as noted previously.

Failure Modes

Figure 7 summarizes the failure modes observed in the GFRP-reinforced wall panels, which were characterized by either rupture of the reinforcement in tension or bond splitting failure. Figure 7(a) shows a typical tensile rupture, which occurred in the specimens with a reinforcement ratio of 0.4 % (3 - #2 GFRP bars) for both epoxy and mortar adhesives, and the failure was characterized by very large displacements in the wall panel and a typical broomstick failure in the GFRP bars (Figure 7(a)). In specimens with a higher reinforcement ratio of 0.6 %, bond splitting failure was observed, which was characterized by longitudinal cracking along the length of the wall panel at the location of the reinforcing bar (Figure 7(b)). Interestingly, the onset of bond failure occurred at significantly different ultimately loads (22.4 kN and 13 kN) and deflections (74 mm and 43 mm) in specimens with epoxy and mortar, respectively, suggesting that the epoxy adhesive provided better bond performance when compared to the mortar as was also indicated earlier in the manuscript.

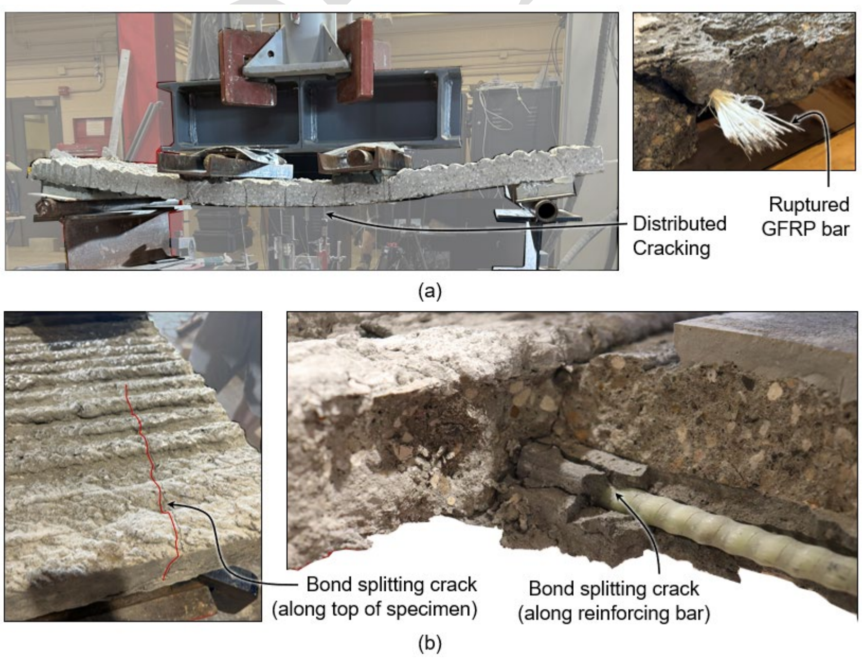

Figure 7. Observed failure modes: (a) rupture of GFRP reinforcement (b) bond splitting failure.

In the steel reinforced specimens, the failure mode was characterized by either yielding of the steel reinforcement or bond failure. In specimens that experienced yielding, failure was typically characterized by large deflections and dilation of cracks along the span with deflection. Yielding was consistently observed in panels that used epoxy to bond the steel NSM reinforcement, even for the larger reinforcement ratio of 1.8%. Both wall panels with a wet-formed groove during printing and bonding of the reinforcement using concrete also experienced a yielding failure. In contrast, specimens that used mortar with steel reinforcement consistently experienced bond failure (with the exception of specimen Steel-0.9-M-1), suggesting once again that the epoxy adhesive or concrete during printing provided improved bond performance when compared to the mortar, as also indicated earlier.

After testing was completed, the panels were saw-cut at midspan in the constant moment region to observe the shape of the groove for the reinforcement and bonding material. Figure 8 shows a set of typical cross-sections of the panels after cutting. The images generally show a high-quality construction process. Both bonding materials were able to consolidate around the bar without any significant voids or discontinuities. Also, the bars were well-centered at roughly half the groove depth. Figure 8(b) shows a cross-section of the steel reinforcement bonded with concrete, the results show that the concrete placed to bond the reinforcement was able to consolidate with the surrounding concrete, as there is no visible evidence of the groove perimeter after cutting. Some discontinuities were observed in the concrete surrounding the bar after cutting, however, both wall panels failed in flexure due to yielding of the steel reinforcement and no bond failure was observed, suggesting that this was not detrimental to performance.

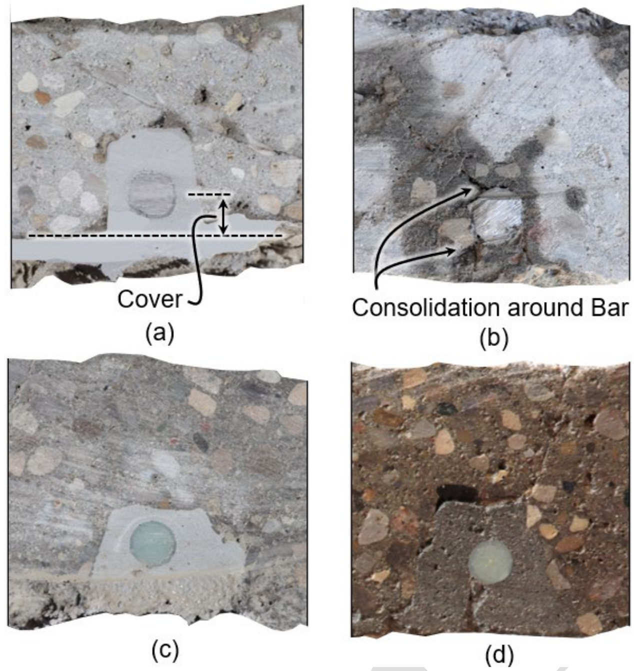

Figure 8. Observed cross-sections of the panels after testing: (a) 10M steel with epoxy, (b) 10M steel with concrete (wet-formed groove), (c) #3 GFRP bar with epoxy, (d) #3 GFRP bar with mortar

Comparison of Crack Spacing

In addition to studying load-displacement behaviour and failure modes, a comparison of the crack distributions throughout the tests is made. Figure 9 shows the typical crack distributions, which were based on manually marked cracks during the test and were comparable amongst nominally identical specimens, and Table 2 summarizes the average crack spacing. The results for the GFRP-reinforced wall specimens, shown in Figure 9(a), show that multiple cracks formed along the length of the panel, suggesting that the bond strength was sufficient to permit distributed cracking. The average crack spacing was similar amongst the specimens with a reinforcement ratio of 0.4 % as well as in the panels that used epoxy to bond the NSM reinforcement. In the panels GFRP-0.6-M, fewer cracks formed along the member length, suggesting that the bond strength was lower, something that was also reflected in the failure mode. Figure 9(b) shows the crack distributions for the steel-reinforced wall panels. Generally, the steel-reinforced panels formed fewer cracks along the member length, which is attributed to the higher reinforcement ratios. This was especially true in the wall panels with the largest reinforcement ratio of 1.8%, which tended to form one or two cracks along the member length.

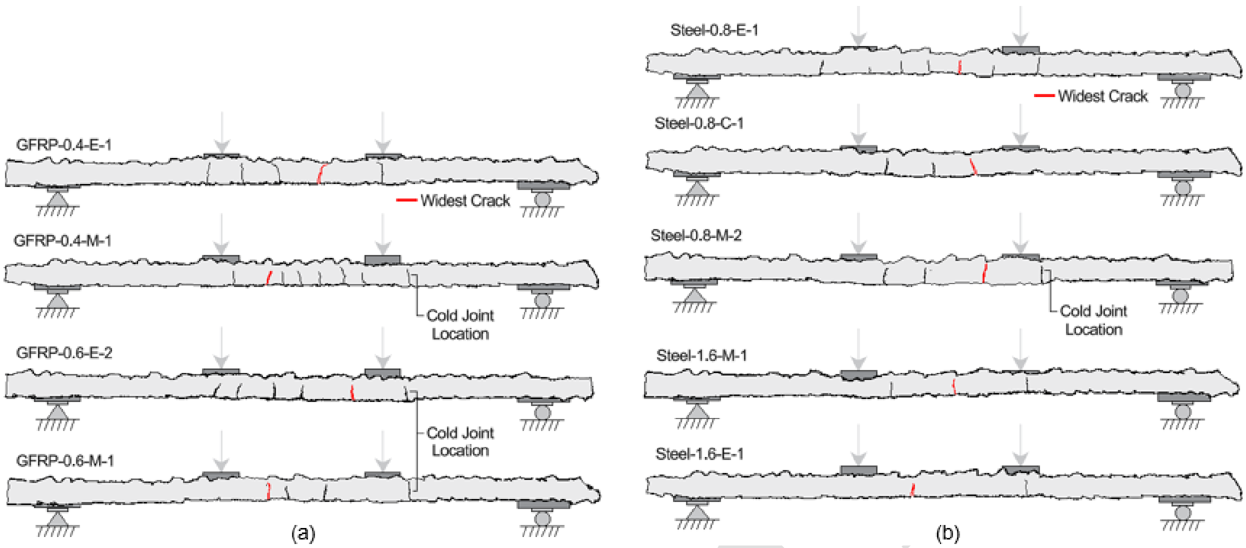

Figure 9. Typical crack distributions for each specimen type: (a) GFRP-reinforced wall panels, (b) steel-reinforced wall panels.

One of the interesting nuances of having a 3DCP element is the layered nature of the structural component as well as the variation in the thickness of the section along the member length, both of which have the potential to influence the formation of cracks along the member length. Figure 10 shows the locations of where cracks formed in two GFRP-reinforced wall panels (GFRP-0.6-E-1 and GFRP-0.6-M-2), as well as the sections of the wall panel that were thinner and the average thickness (in red), similar to the average thickness (in gray), or more than the average thickness (in green). It is noted that these results were typical of most of the specimens tested in this research. The results show that for specimen GFRP-0.6-E-1 (Figure 10(a)), most cracks initiate in locations where the thickness of the panel was less than the average thickness, which makes sense because these sections would have the lowest moment of inertia. These results are similar to the locations that cracks formed at in specimen GFRP-0.6-M-2 (Figure 10(b)), however, fewer cracks formed along the length, which could be attributed to the bond performance of the mortar or the locations of the thinnest sections of the wall panel (i.e., locations shown in red where $h < h_{avg}$).

Ultimately, these results suggest that panel thickness variation and the locations of thinner sections in a printed wall panel influences where the cracks form and potentially how many cracks form along the member length.

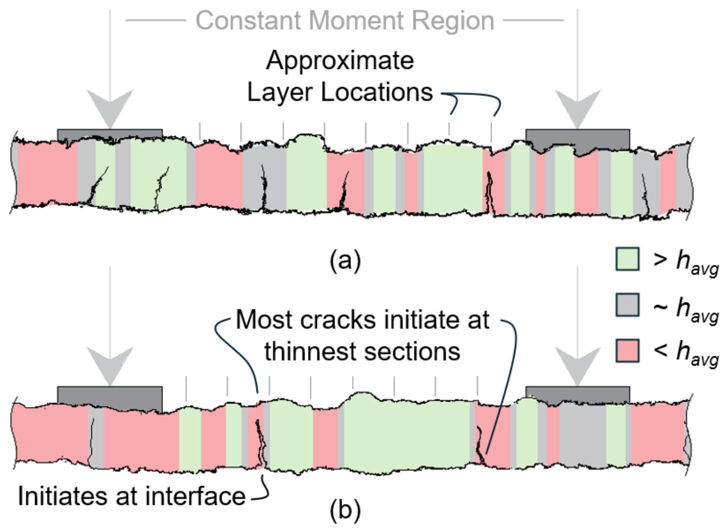

Figure 10. Panel thickness distribution and its influence on crack location in the constant moment region for specimen: (a) GFRP-0.6-E-2 and (b) GFRP-0.6-M-2.

A final observation that can be drawn from the results shown in Figure 10 is the crack formation locations relative to the printed layer interfaces, which are indicated with the short vertical lines above the section (Figure 10). The results show that cracks not only consistently initiated at locations where the member thickness was less than the average thickness of the wall panel (in red), but also they do not necessarily initiate or propagate at the interface between two layers. This is a promising result, as this suggests that the bond strength between layers is not necessarily lower than the tensile strength of the material and thus failure in tension is at the strength of the material, something that was also observed in the modulus of rupture tests.

Analysis of Compression Strains from Digital Image Correlation

One of the key differences in the study of 3DCP structural components compared with traditional reinforced concrete members is the variation in the thickness of the cross-section along the member length, which has implications for the stress distribution in the compression zone. To better understand the distribution of strain, and thus stress, in the compression zone, digital image correlation was used to plot the strain distribution in the constant moment region. Figure 11 shows the distribution of compressive strains through the thickness of two steel-reinforced wall panels (Steel-0.9-M-2 and Steel-1.8-E-1). It is noted that compressive strains are limited to -500 με to visualize the strain gradients through the panel thickness but strains were much higher in some cases (local strain concentrations above -3000 με). The results show that a complex state of strain exists in the compression region of the 3DCP panels. In comparison with a conventional prismatic reinforced concrete beam in which a uniform compression zone would be expected, the results show that the depth of compression varies significantly along the length. Generally, the sections of the specimen that are thicker than the average thickness (i.e., $h > h_{avg}$) carry higher compressive strains. Examining the influence of reinforcement ratio by comparing Figure 11(a) and Figure 11(b), the results show that, as expected, the depth of compression increases, however, the non-uniformity in the strain distributions remains. Given the non-uniformity in the strain distributions, these results lead to questions surrounding the classical assumptions of a rectangular stress block in estimating the flexural strength of a reinforced concrete element, something that is examined in the following subsection of this paper.

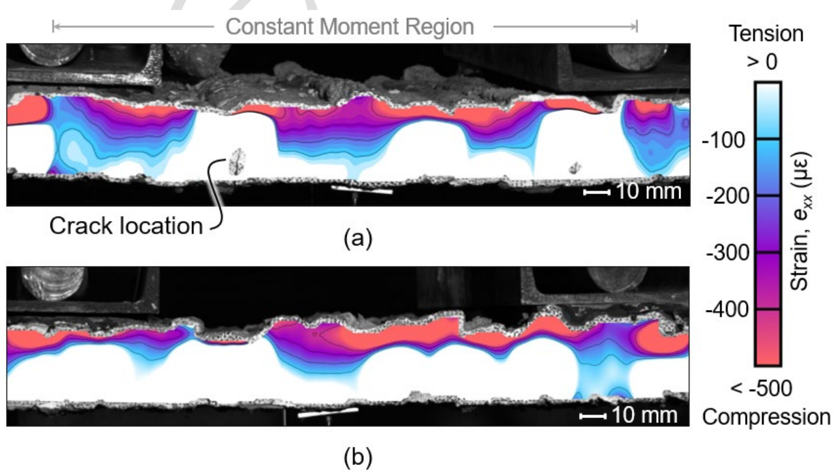

Figure 11. Typical compressive strain distributions in the constant moment region for wall panel: (a) Steel-0.9-M-2 and (b) Steel-1.8-E-1. Tensile strains are shown in white and compressive strains are limited to a maximum value of -500 με.

COMPARISON WITH THEORETICAL PREDICTION OF MOMENT RESISTANCE

The complexity of the strain distribution through the thickness of the wall panel leads to questions about how the theoretical approaches to compute the flexural strength of a reinforced concrete element apply to a 3DCP component with a variable cross-section. To compute the moment resistance, the approach from CSA A23.3:24 [38] is adopted, which is a stress-block approach similar to the approach used by ACI 318-24 [39] except that it assumes a maximum usable compressive strain of 0.0035 in the concrete, as opposed to 0.003. In this approach, the stress block factors are computed using Eq. (1):

$$\begin{aligned} \alpha_1 &= 0.85 - 0.0015 f_c' < 0.87 f_c' \\ \beta_1 &= 0.97 - 0.0025 f_c' < 0.67 f_c' \end{aligned} \tag{1}$$

where f'_c is the compressive strength of the concrete, taken as 44.1 MPa based on material test results. Using equilibrium, the depth to the neutral axis is determined using Eq. (2):

$$c = \frac{\phi_s A_r f_r}{\phi_c \alpha_1 f_c' \beta_1 b} \tag{2}$$

where φ_s and φ_c are material resistance factors, which were taken as 1.0 to compare with experimental results, A_r is the area of longitudinal reinforcement, f_r is the stress in the reinforcement at the ultimate load, and b is the width of the wall panel, which was 600 mm for all specimens in this study. Based on the stress in the reinforcement and the corresponding neutral axis depth, the moment resistance (M_r) is computed based on Eq. (3):

$$M_r = \phi_s A_r f_r (d - \beta_1 c/2) \tag{3}$$

where d is the effective depth of the reinforcement. For the analysis of the wall panels in this study, the cross-section was idealized as a rectangle and the depth of the reinforcement was computed either based on the average thickness of the wall panel (h_{avg} in Table 3) or the minimum thickness (h_{min} in Table 2), using the as-built cover measured for each specimen after testing (sample cross-sections shown in Figure 8). Because the wall panels are comparatively thin the difference in the moment resistance when considering the minimum or average wall panel thickness is significant (can change the moment resistance by 25 % or more).

Based on the procedure outlined in Eq. (1)-(3), a key parameter required to calculate the moment-resistance of the specimens is the stress in the reinforcement (f_r) at the ultimate load. For the steel reinforced panels, the stress in the steel reinforcement was assumed to be equal to the yield stress, as shown in Table 1. It is noted that even for the steel-reinforced wall panels that experienced a bond failure, this failure occurred at a comparable load (within 5 %) to nominally identical specimens that exhibited a distinct yield plateau, as shown in Figure 6, and consequently, it was assumed the reinforcement was near its yield stress in all cases.

For the GFRP reinforced wall panels that failed due to rupture of the reinforcement, it was assumed that the bars reached their ultimate tensile strength (i.e., GFRP-0.4-E and GFRP-0.4-M). For these specimens, CSA S806:22 [40] was used to determine if the stress block approach could be used to evaluate the strength of the panels, which depends on the inequality in Eq. (4):

$$\frac{c}{d} \leq \frac{7}{7 + 2000\epsilon_{Fu}} \tag{4}$$

where is the ultimate tensile strain in the GFRP reinforcement, which was assumed to be 1.7 %. Ultimately, the panels did not meet this criterion, and so, the stress in the concrete was assumed to be linearly distributed and the forces in the GFRP and concrete were based on compatibility conditions. In the other GFRP reinforced specimens that experienced a bond failure, the stress in the reinforcement at failure is difficult to estimate without strain measurements on the reinforcement. While some researchers have proposed methods to predict reinforcement strain using surface crack width measurements [41-42], this depends on an assumed bond-slip model for the reinforcement, amongst other factors, which leads to uncertainty surrounding the results and varying degrees of effectiveness have been reported in the literature [41-42]. Consequently, these panels were not analyzed in this study.

Table 3 summarizes the predicted moment resistance computed using the minimum ($M_{p,min}$) and the average ($M_{p,avg}$) wall panel thickness and compares the results with the experimentally measured moment resistance (M_{exp}). The results show that the experimental moment resistance consistently falls between the predicted moment resistance based on the minimum (h_{min}) and average (h_{avg}) cross-section thickness. When the minimum thickness is used to predict the moment resistance, it consistently underestimates the flexural strength by approximately 25 % on average (COV = 0.13), suggesting that this will produce conservative results. Alternatively, while closer to the observed experimental results, the use of the average thickness has a tendency to overestimate the moment resistance, as the average ratio of the predicted to experimental moment resistance was 1.08 (COV = 0.16). These results highlight the complexity in determining the flexural strength of 3DCP wall panels, especially those with very thin cross-sections. Based on the results of this study, a design thickness (h_{design}) is proposed, which results in an M_n/M_{exp} ratio close to unity. Based on the analysis, a design thickness of $h_{design} = 0.4h_{min}+0.6h_{avg}$ is proposed, which results in a predicted-to-test ratio $M_n/M_{exp} = 1$ (COV = 0.12).

Table 3. Comparison of experimental and theoretical moment resistance based on minimum (h_{min}) or average panel thickness (h_{avg})

Specimen Name	h_{min} (mm)	h_{avg} (mm)	M_{exp} (kNm)	$M_{p,min}$ (kNm)	$\frac{M_{p,min}}{M_{exp}}$	$M_{p,avg}$ (kNm)	$\frac{M_{p,avg}}{M_{exp}}$
GFRP-0.4-E	50	62	3.22	2.73	0.92	3.85	0.72
GFRP-0.4-M	45	59	3.77	2.95	0.72	3.78	1.00
Steel-0.9-E-1	46	59	4.55	4	0.88	5.27	1.18
Steel-0.9-E-2	38	51	4.32	3.47	0.8	4.60	1.10
Steel-0.9-C-1	48	60	4.51	3.72	0.83	5.12	1.09
Steel-0.9-C-2	44	57	3.48	3.76	1.08	4.83	1.44
Steel-0.9-M-1	47	58	4.32	3.49	0.81	5.06	1.09
Steel-0.9-M-2	48	56	4.06	3.15	0.78	3.97	0.95
Steel-1.8-E-1	42	57	8.53	6.05	0.71	10.0	1.06
Steel-1.8-E-2	43	55	7.61	6.69	0.88	10.2	1.20
Steel-1.8-M-1	38	54	6.73	4.42	0.66	6.86	1.05
Steel-1.8-M-2	44	54	6.59	5.73	0.87	7.62	1.12
				Average	0.83		1.08
				COV	0.13		0.16

CONCLUSIONS

This paper presents the results of an experimental study on the structural behaviour of single-wythe 3DCP wall panels with NSM reinforcement under out-of-plane loads. The influence of groove type, including a newly introduced approach (saw-cut versus wet-formed), reinforcement type (steel and GFRP), and material used to bond the NSM reinforcement in the groove (epoxy, mortar, and the same printed concrete) were investigated. Overall, results of the study demonstrate that NSM reinforcement is effective at improving the flexural strength of 3DCP wall panels and that behaviour similar to that of conventional reinforced concrete members, even in a thin printed wythe, can be achieved. The specific conclusions of this study include:

1. Newly developed wet-formed grooves were found to be a very efficient approach to installing NSM reinforcement in 3DCP wall during construction. A custom trowel is proposed to aid in the formation of these grooves and the results showed that the groove could be formed in a matter of minutes. This approach could be automated in future work (e.g., using a robotic arm), and by using the same print material to bond the NSM reinforcement, this represents a fully autonomous approach to incorporating longitudinal reinforcement in 3DCP structures.
2. Steel reinforcement of 0.9% and 1.8% reinforcement ratios installed in both saw-cut and wet-formed grooves consistently achieved ductile flexural failure, including yielding of steel reinforcement, irrespective of whether printing material, epoxy, or cementitious mortar were used to bond the reinforcement.
3. GFRP-reinforced wall panels with a reinforcement ratio of 0.4% failed due to rupture of the GFRP reinforcement at the maximum load. At a higher reinforcement ratio of 0.6%, the specimens experienced sudden bond failure at the maximum load for both epoxy and mortar bond materials, however, the specimens that used epoxy adhesive had approximately 1.4 times higher load carrying capacity when compared to those that used cementitious mortar, suggesting that epoxy can provide better bond performance.
4. 3DCP wall panels has a significant inherent variability in wythe thickness (of up to 15 % in this study) due to the additive manufacturing process. This in turn led to high variability in cracking load amongst the tested wall panels. Cracks were consistently found to form at the thinnest sections and propagated

through the print material rather than through the layer-to-layer interface, suggesting adequate bond between layers.

5. Theoretical methods used in design codes to predict the flexural strength of the wall panels using an equivalent stress block approach were found to be capable of estimating the flexural strength with reasonable accuracy. The experimentally measured moment-resistance consistently fell within the predicted resistance computed using the minimum (h_{min}) and average (h_{avg}) wythe thickness. Results suggest that the use of the average thickness will produce results that are close to those observed experimentally, while use of the minimum thickness would result in conservative strength estimates. A design thickness ($h_{design} = 0.4h_{min} + 0.6h_{avg}$) is proposed.
6. Digital image correlation showed that a complex state of strain exists in the compression zone of 3DCP elements, particularly thin wythes, stemming from the variability in the layer thickness along the panel length.

DATA AVAILABILITY STATEMENT

Some or all data, models, or code that support the findings of this study are available from the corresponding author upon reasonable request.

ACKNOWLEDGEMENTS

The authors gratefully acknowledge the financial support of the Federal Government of Canada (grant number RKI-1434). The material donation and technical assistance from nidus3D, VROD, Sika, and MST Bar are also gratefully acknowledged. Technical assistance in the laboratory from Justin Bennett and Hal Stephens are also acknowledged.

NOMENCLATURE

A_r	Area of longitudinal reinforcement (mm^2)
A_b	Area of reinforcing bar (mm^2)
b	Panel width (mm)
c	Depth of compression (mm)
d_b	Diameter of reinforcing bar (mm)
d	Nominal effective depth (mm)
d_{min}	Effective depth based on h_{min} (mm)
d_{avg}	Effective depth based on h_{avg} (mm)
f'_c	Concrete compressive strength (MPa)
f_r	Stress in the reinforcing bar (MPa)
f_y	Yield stress (MPa)
h	Nominal wythe thickness (mm)
h_{min}	Minimum wythe thickness (mm)
h_{avg}	Average wythe thickness (mm)
k_i	Initial stiffness (kN/mm)
M_{exp}	Experimentally measured moment resistance (kNm)
$M_{p,min}$	Predicted moment resistance based on h_{min} (kNm)
$M_{p,avg}$	Predicted moment resistance based on h_{avg} (kNm)
M_r	Moment resistance (kNm)
P_{cr}	Cracking load (kN)
P_{max}	Maximum load (kN)
s_{avg}	Average crack spacing (mm)
α_1	Stress block parameter
β_1	Stress block parameter
φ_s	Steel material resistance factor
φ_c	Concrete material resistance factor
Δ_y	Yield displacement (mm)
Δ_{ult}	Ultimate displacement (mm)
ρ	Reinforcement ratio (%)

REFERENCES

[1] Brozovsky, J., Labonnote, N., & Vigren, O. (2024). Digital technologies in architecture, engineering, and construction. Automation in Construction, 158, 105212.

[2] El-Sayegh, S., Romdhane, L., & Manjikian, S. (2020). A critical review of 3D printing in construction: benefits, challenges, and risks. Archives of civil and mechanical engineering, 20(2), 34.

[3] Mohamed, R. A., & Mohamed, A. F. A. (2025). Exploring the environmental benefits of 3D printing technology in concrete construction; a review. Progress in Additive Manufacturing, 10(1), 279-289.

[4] Zhang, J., Wang, J., Dong, S., Yu, X., & Han, B. (2019). A review of the current progress and application of 3D printed concrete. Composites Part A: Applied Science and Manufacturing, 125.

[5] Heidarnezhad, F., and Zhang, Q. (2022). Shotcrete based 3D concrete printing: State of art, challenges, and opportunities. Construction and Building Materials, 323, 126545.

[6] Cai, J., Wang, J., Zhang, Q., Du, C., Meloni, M., and Feng, J. (2024). State-of-the-art of mechanical properties of 3D printed concrete. Case Studies in Construction Materials, 21.

[7] Han, X., Yan, J., Liu, M., Huo, L., & Li, J. (2022). Experimental study on large-scale 3D printed concrete walls under axial compression. Automation in Construction, 133, 103993.

[8] Silveira, M. V., Wagner, J. S., Khanverdi, M., & Das, S. (2024). Structural performance of large-scale 3D-printed walls subjected to axial compression load. Canadian Journal of Civil Engineering, 51(8), 919-933.

[9] Khanverdi, M., & Das, S. (2025). Performance of full-scale 3D-printed concrete walls: Effects of vertical reinforcements and window opening. Engineering Structures, 337, 120510.

[10] Wang, J., Zhang, P., Feng, J., & Cai, J. (2024). Experimental study and design approach on 3D printed concrete walls under eccentric axial compression. Case Studies in Construction Materials, 20, e02892.

[11] Delavar, M. A., Chen, H., & Sideris, P. (2024). Analysis and design of 3D printed reinforced concrete walls under in-plane quasi-static loading. Engineering Structures, 303, 117535.

[12] Liu, C., Liang, Z., Liu, H., Wu, Y., Zhang, Y., & Bai, G. (2025). Seismic performance of 3D printed reinforced concrete walls: Experimental study and numerical simulation. Engineering Structures, 333, 120176.

[13] Aghajani Delavar, M., Sharma, S., Chen, H., Sideris, P., & Kreiger, E. (2026). Experimental Investigation on Full-Scale Shear-Critical 3D Printed Concrete Walls Subjected to In-Plane Cyclic Loading. Journal of Structural Engineering, 152(4), 04026019.

[14] Sritharan, S., Beyer, K., Henry, R. S., Chai, Y. H., Kowalsky, M., & Bull, D. (2014). Understanding poor seismic performance of concrete walls and design implications. Earthquake Spectra, 30(1), 307-334.

[15] Bruneau, M. (1994). State-of-the-art report on seismic performance of unreinforced masonry buildings. Journal of structural engineering, 120(1), 230-251.

[16] Ferreira, T. M., Costa, A. A., & Costa, A. (2015). Analysis of the out-of-plane seismic behavior of unreinforced masonry: A literature review. International Journal of Architectural Heritage, 9(8), 949-972.

[17] Wu, Z., Memari, A. M., and Duarte, J. P. (2022). State of the art review of reinforcement strategies and technologies for 3D printing of concrete. Energies, 15(1), 360.

[18] Kloft, H., Empelmann, M., Hack, N., Herrmann, E., & Lowke, D. (2020). Reinforcement strategies for 3D-concrete-printing. Civil Engineering Design, 2(4), 131-139.

[19] Asprone, D., Auricchio, F., Menna, C., & Mercuri, V. (2018). 3D printing of reinforced concrete elements: Technology and design approach. Construction and building materials, 165, 218-231.

[20] Buswell, R. A., De Silva, W. L., Jones, S. Z., & Dirrenberger, J. (2018). 3D printing using concrete extrusion: A roadmap for research. Cement and concrete research, 112, 37-49.

[21] Classen, M., Ungermann, J., & Sharma, R. (2020). Additive manufacturing of reinforced concrete—development of a 3D printing technology for cementitious composites with metallic reinforcement. Applied sciences, 10(11), 3791.

[22] Scott, C. (2016). Chinese Construction Company 3D Prints an Entire Two-Story House On-Site in 45 Days—3DPrint.com: The Voice of 3D Printing/Additive Manufacturing. (17 June 2016). Available online: https://3dprint.com/138664/huashang-tengda-3d-printhouse/ (accessed on March 3 2026).

[23] Hack, N., Lauer, W. V., Gramazio, F., & Kohler, M. (2014). Mesh-mould: Differentiation for enhanced performance. In Rethinking Comprehensive Design: Speculative Counterculture, Proceedings of the 19th International Conference on Computer-Aided Architectural Design Research in Asia (CAADRIA'14) (pp. 139-148). CAADRIA.

[24] Mechtcherine, V., Grafe, J., Nerella, V. N., Spaniol, E., Hertel, M., & Füssel, U. (2018). 3D-printed steel reinforcement for digital concrete construction–Manufacture, mechanical properties and bond behaviour. Construction and Building Materials, 179, 125-137.

[25] Kreiger, E. L., Kreiger, M. A., & Case, M. P. (2019). Development of the construction processes for reinforced additively constructed concrete. Additive Manufacturing, 28, 39-49.

[26] Sylaj, V., Fam, A., Hachborn H., and Burak, R. (2020). Flexural response of double-wythe insulated ultra-high-performance concrete panels with low to moderate composite action, PCI Journal, 65(1):24-40.

[27] Zhang, S. S., Yu, T., & Chen, G. M. (2017). Reinforced concrete beams strengthened in flexure with near-surface mounted (NSM) CFRP strips: Current status and research needs. Composites Part B: Engineering, 131, 30-42.

[28] Inkscape Project (2025). Inkscape. Retrieved from https://inkscape.org

[29] Wagner, J. S., Silveira, M. V., Vanderlei, R. D., & Das, S. (2024). Comparative analysis of mold-cast and 3D-printed cement-based components: implications for standardization in additive construction. Canadian Journal of Civil Engineering, 52(4), 388-404.

[30] ASTM International (2023). ASTM C39/C39M-23: Standard Test Method for Compressive Strength of Cylindrical Concrete Specimens. ASTM International, West Conshohocken, PA.

[31] ASTM International (2022). ASTM C78/C78M-22: Standard Test Method for Flexural Strength of Concrete (Using Simple Beam with Third-Point Loading). ASTM International.

[32] Sika (2023). Sika MonoTop-623 F: Product data sheet. Sika Canada Inc. Accessed from: https://can.sika.com/dam/dms/ca01/g/sika-monotop-623f.pdf

[33] Sika (2025). Sikadur-30: Product data sheet (Version 04.01). Accessed from: https://can.sika.com/dam/dms/ca01/4/sikadur-30.pdf

[34] Pultrall Inc. (2025). V-ROD Grade I Glass Fiber Reinforced Polymer (GFRP) rebar: Technical data sheet [Technical datasheet]. Accessed from: https://fiberglassrebar.com

[35] MST Rebar Inc. (2024). MST-BAR: Structural and Flat Work GFRP rebar technical data. MST Rebar Inc. Accessed from: https://mstbar.com/products/technical-data

[36] ASTM International (2024). ASTM E8/E8M-24: Standard Test Methods for Tension Testing of Metallic Materials. ASTM International. Accessed from: https://www.astm.org/Standards/E8_E8M.htm

[37] Correlated Solutions (2026). Non-contact, full-field strain, and deformation measurement system. Available from: https://www.correlatedsolutions.com/vic-3d. [Accessed March 4, 2026]

[38] CSA A23.3:24, Design of concrete structures, CSA Group, 2024.

[39] ACI 318-25, Building Code Requirements for Structural Concrete (ACI 318-25) and Commentary, American Concrete Institute, 2025.

[40] CSA S806:22, Design and construction of building structures with fibre-reinforced polymers, CSA Group, 2022.

[41] Carmo, R. N. F., Valença, J., Silva, D., & Dias-Da-Costa, D. (2015). Assessing steel strains on reinforced concrete members from surface cracking patterns. Construction and Building Materials, 98, 265-275.

[42] Brault, A., & Hoult, N. A. (2019). Distributed Reinforcement Strains: Measurement and Application. ACI Structural Journal, 116(4).